energies

MDPI

Article

Optimization of an Organic Rankine Cycle–Vapor Compression Cycle System for Electricity and Cooling Production from Low-Grade Waste Heat

Łukasz Witanowski

Turbine Department, Institute of Fluid-Flow Machinery, Polish Academy of Sciences, 80-231 Gdańsk, Poland; lwitanowski@imp.gda.pl

Abstract: In light of the intensifying global climate crisis and the increasing demand for efficient electricity and cooling systems, the exploration of advanced power generation technologies has become crucial. This paper presents a comprehensive analysis of Organic Rankine Cycle–Vapor Compression Cycle (ORC-VCC) systems utilizing low-grade waste heat for the dual purpose of electricity and cooling production. The study focuses on systems that harness waste heat below 90 °C with thermal inputs up to 500 kW. An in-house Python code was developed to calculate cycle parameters and perform multi-objective optimization targeting the maximization of both ORC-VCC efficiency and power output. The optimization was conducted for 10 different cases by evaluating five working fluids across two different ambient temperatures. The analysis reveals that the optimized system achieved an impressive overall cycle efficiency exceeding 90%, demonstrating the significant potential of ORC-VCC technology in waste heat recovery applications. The Non-Dominated Sorting Genetic Algorithm II (NSGA-II) multi-objective optimization approach was found to be particularly effective at navigating the multi-dimensional solution space and identifying the global optimum. This study provides valuable insights into system performance across a range of operating conditions and design parameters. Sensitivity analyses highlight key factors influencing cycle efficiency and power output. These findings have important implications for the development and deployment of ORC-VCC systems as a sustainable and efficient solution to meet growing energy needs while reducing greenhouse gas emissions.

Keywords: Organic Rankine Cycle; Vapor Compression Cycle; waste heat; multi-objective optimization; Non-Dominated Sorting Genetic Algorithm II

Citation: Witanowski, Ł. Optimization of an Organic Rankine Cycle–Vapor Compression Cycle System for Electricity and Cooling Production from Low-Grade Waste Heat. *Energies* **2024**, *17*, 5566. https://doi.org/10.3390/en17225566

Academic Editor: George Kosmadakis

Received: 2 October 2024
Revised: 29 October 2024
Accepted: 29 October 2024
Published: 7 November 2024

1. Introduction

The pressing challenges posed by the climate crisis and escalating global energy consumption call for innovative approaches to enhance energy efficiency and promote sustainability. The rising global surface temperature is a significant determinant of future demand for air cooling installations, as elevated temperatures directly correlate with increased cooling requirements to maintain comfortable indoor environments. Figure 1 illustrates the real and projected global surface temperature increases from 1900 to 2100 under various greenhouse gas emission scenarios, as estimated by climate models [1]. The figure illustrates three distinct warming trajectories, designated as high growth (A2), moderate growth (A1B), and low growth (B1), which represent scenarios based on varying levels of fossil fuel consumption and greenhouse gas emissions. The shaded regions indicate the variability between models and the uncertainty range of temperature predictions. Additionally, a scenario in which CO_2 concentrations remain constant at 2000 levels is illustrated. The models project that by 2100, the global average surface temperature could increase by approximately 2 °C to over 4 °C, depending on the rate of greenhouse gas emissions. This underscores the vital necessity of emission mitigation to restrict future warming and the subsequent surge in energy demands for air conditioning.

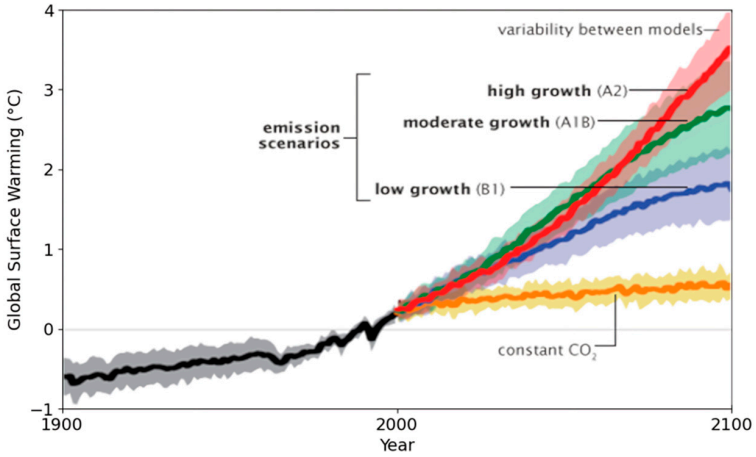

Figure 1. Projected global surface warming under different emission scenarios [1].

As illustrated in the preceding figure, the rising global temperatures are anticipated to exert a considerable impact on the demand for air cooling installations. Figure 2 presents the projected growth in the total number of air cooling devices from 1990 to 2050, disaggregated by various global regions [2]. The data demonstrate a gradual increase in the uptake of air cooling systems, particularly in the period following 2020, as a response to rising global temperatures. The projections indicate that by the year 2050, the number of air cooling devices in use worldwide will exceed 5.5 billion units. The United States is shown to have a significant early adoption of air cooling devices, but, over time, there is a notable shift towards rapid growth in China and other emerging economies, including India, Indonesia, and the Middle East. China is projected to experience the most rapid growth, eventually surpassing the United States by 2050. Additionally, other regions, including the European Union, Japan, Korea, and emerging economies, such as Brazil, Mexico, and Indonesia, are also anticipated to demonstrate a notable increase in the adoption of air conditioning systems. The "rest of the world" category is projected to constitute a significant proportion of the total by 2050, indicating a pervasive adoption of these technologies across developing regions. This trend indicates that the global increase in temperature is resulting in an elevated demand for cooling solutions, particularly in emerging markets that previously had limited access to such technologies. These projections underscore the growing energy demand associated with cooling and highlight the necessity of the development of energy-efficient cooling technologies and policies to mitigate the impact on greenhouse gas emissions.

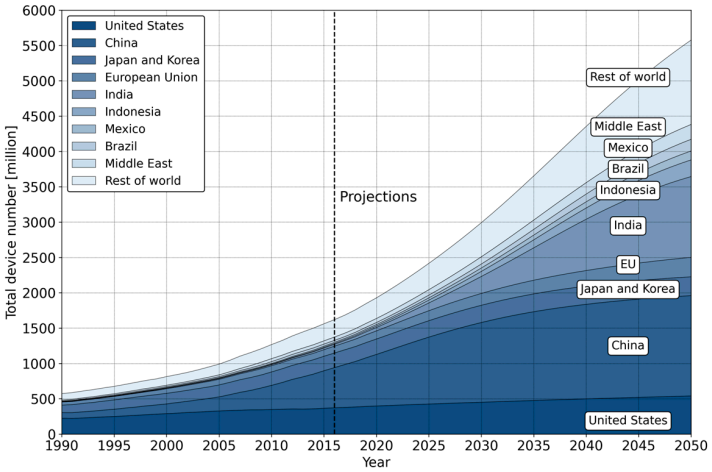

Figure 2. Growth in global air conditioner stock, 1990–2050.

One method for reducing electricity demand is the utilization of waste heat, which is generated during the majority of energy conversion processes and is frequently discarded into the environment. To enhance process efficiencies, it is imperative to identify viable solutions for the repurposing of waste heat. The bar chart (Figure 3) illustrates the distribution of waste heat across sectors, namely transportation, residential, commercial, industrial, and electricity generation [3]. The sectors are categorized by temperature ranges: low (less than 100 °C), medium (100–299 °C), and high (equal to or greater than 300 °C). The electricity generation sector is responsible for the majority of low-temperature waste heat production (88%), which presents a significant opportunity for recovery. Globally, the majority of waste heat is classified as low-grade (63%), followed by high-grade (21%) and medium-grade (16%). The treemap (Figure 4) provides further detail regarding the potential for low-grade waste heat utilization across different sectors. The largest opportunity for energy recovery is in electricity generation, with 26.21 TWh of low-grade waste heat available, followed by the transportation sector with 7.91 TWh. The industrial, residential, and commercial sectors contribute 3.72 TWh, 3.04 TWh, and 2.34 TWh, respectively. These figures highlight the significant potential of energy recovery, particularly in electricity generation and transportation, to enhance energy efficiency and reduce electricity demand.

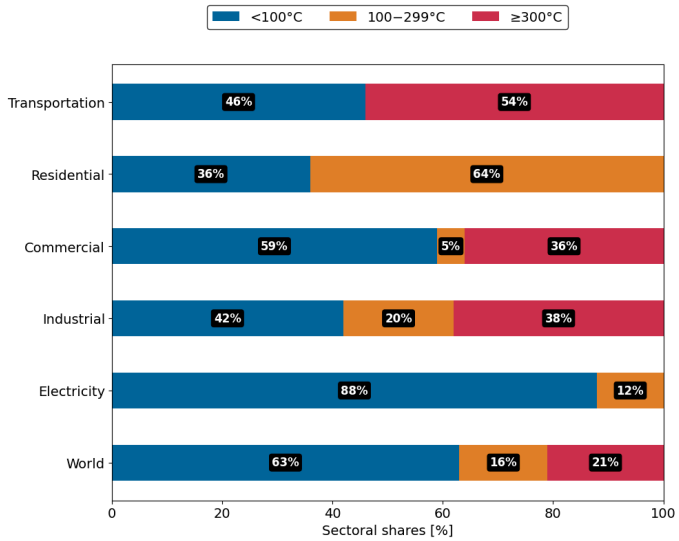

Figure 3. Sectoral shares in low-grade waste heat.

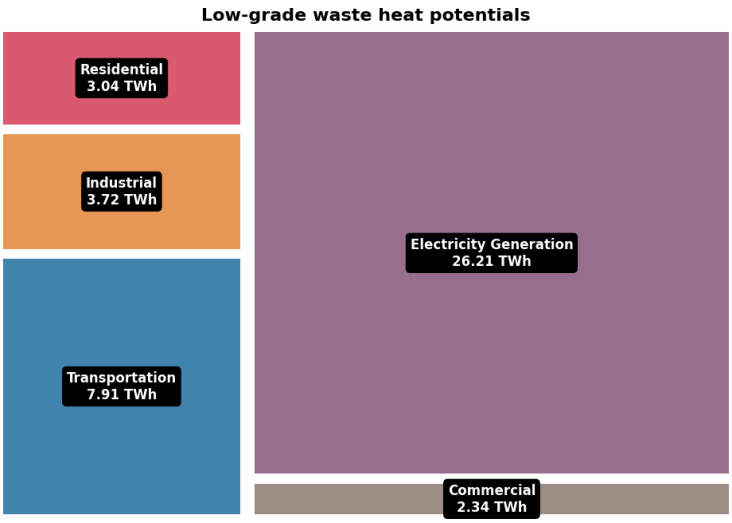

Figure 4. Low-grade waste heat potentials.

In light of these developments, thermodynamic cycles, such as the Organic Rankine Cycle (ORC) and the Vapor Compression Cycle (VCC), have been extensively utilized in a multitude of industrial contexts. The ORC [4,5] is primarily utilized for energy conversion, particularly in the context of waste heat recovery, whereas the VCC [6–8] is employed in refrigeration systems. ORC technology is a mature technology with a substantial body of scientific literature [9,10]. Recently, the combination of these two cycles into an integrated ORC-VCC system has attracted the attention of both academic researchers and industry experts. This attention is a consequence of the system's promising capability of achieving greater energy efficiency and effective waste heat utilization. The integrated ORC-VCC system not only streamlines the traditional configurations of each cycle but also leverages the synergies between them. This is illustrated in the system's elementary configuration, depicted in Figure 5.

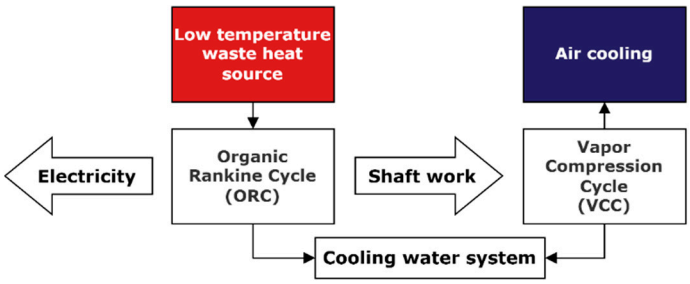

Figure 5. Conception of ORC-VCC [11].

Analyses pertaining to ORC-VCC encompass a multitude of considerations. The construction of the system is a key consideration, with analyses conducted on both the inclusion [11] and the exclusion [12,13] of an ORC regenerator. Furthermore, the analyses include calculations and comparisons of the primary parameters that define the cycle for a single working medium [14], as well as for multiple working fluids [11–13,15]. Advanced systems are also considered, including those comprising multiple compressors [15] operating within a single cycle (i.e., not separated) [14–17] and those powered by solar [18] or hybrid sources [19]. Of particular significance are the analyses that present system parameters for various operating parameters, with results obtained through calculation [20,21] or experimentation [22–24].

The objective of this research is to perform a multi-objective optimization of a 500 kW thermal input power ORC-VCC system, with a specific focus on integrating five low-GWP refrigerants and two ambient temperatures (15 °C and 30 °C). The lower temperatures provide insight into the potential maximum COP of the analyzed working fluids. Moreover, this study employs a more realistic assumption regarding the condenser inlet temperature, setting it at 30 °C. This adjustment more accurately reflects the conditions anticipated in a warming climate for cooling applications. By incorporating a higher inlet temperature, the model more precisely captures the operational challenges introduced by climate change, thereby facilitating a more effective and comprehensive optimization process. In such a scenario, we can compare the optimization results for two extreme operating temperatures of the system. Additionally, there is a notable absence in the existing literature regarding the optimization of ORC-VCC system parameters, particularly with regard to the exploration of multiple degrees of freedom and the testing of various objective functions. The majority of studies have concentrated on a limited number of parameters, frequently neglecting the intricate interactions between the various components of the system. This research addresses these shortcomings by employing a comprehensive, multi-objective optimization approach incorporating multiple degrees of freedom and evaluating a range of objective functions.

2. ORC-VCC Model Optimization Methodology

2.1. System Description and Parameters

The schematic of the thermodynamic cycle of the ORC-VCC system is shown in Figure 6. The system consists of an ORC with a regenerator subsystem and a VCC subsystem. The cycle was analyzed using a single working fluid while ensuring that the same fluid was used in both the ORC and the VCC cycles throughout the study. Furthermore, the present study incorporates the potential for electricity generation, which was not included in the previous investigation [11]. The assumptions related to the system are detailed in Table 1. The efficiencies of the machines were selected with a significant safety margin. The internal efficiencies of both the compressor and the turbine were conservatively set at 80%. The assumed values are lower than those typically reported in the recent literature for similar low-power turbomachinery.

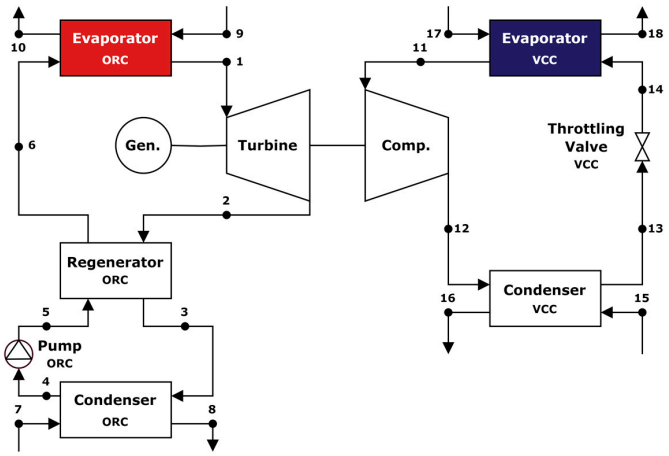

Figure 6. Schematic diagram of the ORC-VCC with electricity generation [11].

Table 1. Efficiency and thermodynamic assumptions of the ORC-VCC system.

Parameter	Symbol	Unit	Value
Chilled water temperature (cold side)	T_{18}	°C	8
Chilled water temperature (hot side)	T_{17}	°C	12
Cooling water temperature (cold side)	T_7, T_{15}	°C	15 and 30
Heat source mass flow	m_9	kg/s	8.5
Heat source temperature (hot side)	T_9	°C	89.3
Compressor efficiency (VCC)	η_c	-	80%
Pump efficiency (ORC)	η_p	-	50%
Turbine efficiency (ORC)	η_t	-	80%

2.2. Optimization Approach

The optimization methodology for this study integrates advanced multi-objective optimization techniques using the pymoo library [25], a versatile Python framework for multi-objective optimization, alongside a custom-developed code to accurately model and evaluate the performance of a small-scale ORC-VCC system. This combined approach enables the precise and efficient exploration of the solution space while addressing the complexity of the system's design parameters and objectives.

The ORC-VCC system is modeled using a custom code developed specifically for this study. This code simulates the thermodynamic behavior of the system, thus allowing for the evaluation of key performance indicators. The problem is formulated with 13 decision variables that directly influence the system's behavior, and each is bounded within specified limits (lower bounds of 0.1 to 50 and upper bounds of 10 to 85). These variables capture the essential parameters that affect the system's overall performance. A detailed overview of these variables is presented in Table 2.

Table 2. Decision variables and their boundaries for the ORC-VCC system's optimization.

Arg.	Parameter	Symbol	Unit	Lower Bounds	Upper Bounds
x_1	Evaporator pinch temperature difference (VCC)	ΔT_{vcc_ev}	°C	3	10
x_2	Degree of superheating in evaporator (VCC)	ΔT_{vcc_sup}	°C	3	10
x_3	Degree of subcooling in condenser (VCC)	ΔT_{vcc_sub}	°C	3	10
x_4	Regenerator pinch temperature difference (ORC)	ΔT_{orc_reg}	°C	3	15
x_5	Degree of superheating in evaporator (ORC)	ΔT_{orc_sup}	°C	3	15
x_6	Degree of subcooling in condenser (ORC)	ΔT_{orc_sub}	°C	7	15
x_7	Evaporator pinch temperature difference (ORC)	ΔT_{orc_ev}	°C	3	10
x_8	Condenser pinch temperature difference (ORC)	ΔT_{orc_con}	°C	3	10
x_9	Saturation temperature in evaporator (ORC)	T_{1sv}	°C	50	85
x_{10}	Saturation temperature in condenser (ORC)	T_{4sv}	°C	25	55
x_{11}	Chilled water mass flow rate (VCC)	m_{16}	kg/s	0.1	30
x_{12}	Pressure on the inlet of the compressor (VCC)	p_{12}	bar	0.1	10
x_{13}	Condenser pinch temperature difference (VCC)	ΔT_{vcc_con}	°C	3	10

The optimization process targets two primary objectives:

- Objective Function 1: Maximizing the Coefficient of Performance (COP), a critical measure of the system's efficiency when converting energy input into cooling output.

$$f_1 = COP = \frac{Q_{vcc\_evaporator}}{Q_{orc\_evaporator}} \quad (1)$$

- Objective Function 2: Maximizing the power netto, which is generated by the turbine (P_{turb}) after accounting for the power required by the compressor (P_{comp}). This ensures that the system can deliver the highest possible net electrical performance while fully covering the energy demand of the compressor.

$$f_2 = P_{netto} = P_{turb} - P_{comp} \quad (2)$$

The optimization tasks are executed using the pymoo library, which has been selected for its robust capabilities in addressing multi-objective optimization problems. pymoo offers comprehensive support for a diverse range of evolutionary algorithms, including the Non-Dominated Sorting Genetic Algorithm II (NSGA-II) [26,27], which has been utilized in this study. The optimization tasks are executed using the pymoo library, which has been selected on the basis of its particular suitability for the handling of multi-objective optimization problems. Pymoo supports a range of evolutionary algorithms, including the Non-Dominated Sorting Genetic Algorithm III (NSGA-III) [28], which is specifically designed to efficiently search for and maintain a diverse set of optimal solutions. This makes it an ideal choice for complex multi-objective problems where the trade-offs between objectives need to be thoroughly explored. The algorithm was successfully applied in several case studies, including the energy-efficient retrofit of urban residential buildings and the sustainable renovation of commercial office spaces [29]. These case studies demonstrate the effectiveness of the algorithm in balancing environmental, economic, and social objectives. An additional example is the Organic Rankine Cycle (ORC) for a hybrid solar–waste energy plant [30], whereby the integration of the ORC with solar and waste heat sources results in enhanced exergy efficiency and elevated initial investment costs. This illustrates the trade-off between enhanced system performance and investment expenses. Another illustrative example of the application of the NSGA is in the optimization of a solar-powered combined cooling, heating, and power (CCHP) energy system with phase-change material and water electrolysis [31]. In this application, the NSGA was employed for the purpose of performing a thermoeconomic assessment and optimization of the system. The algorithm simultaneously considered multiple objectives, including cost minimization, efficiency maximization, and environmental impact reduction. By handling the complex trade-offs

between these objectives, NSGA enabled researchers and engineers to identify optimal configurations that enhance the overall performance of the energy system. This resulted in a design that not only improves energy efficiency but also reduces operational costs and minimizes environmental footprints, demonstrating the algorithm's effectiveness in optimizing advanced thermodynamic systems. A notable illustration of the application of the NSGA-II is in the optimization of a Simple Organic Rankine Cycle (SORC) and a Recuperative Organic Rankine Cycle (RORC) system [32]. Researchers employed the NSGA-II in conjunction with the TOPSIS method to simultaneously enhance several performance metrics: thermal efficiency and the power output per unit heat transfer area, the electricity production cost, the equivalent carbon dioxide emission, and the unit electricity production cost. This application demonstrates the effectiveness of the NSGA-II at balancing multiple competing objectives in complex energy systems.

The optimization process is initialized by defining the problem through the class, where the custom code for ORC-VCC system calculations is embedded within the evaluation function. This function is called during each iteration of the optimization to assess the performance of each candidate solution according to the two objectives. The study systematically examines ten cases, each defined by a different combination of low-GWP refrigerants and cooling water temperature:

- a1: R1233zd with cooling water at 15 °C (T_7 and T_{15}).
- a2: R1244yd with cooling water at 15 °C (T_7 and T_{15}).
- a3: R1336mzz with cooling water at 15 °C (T_7 and T_{15}).
- a4: R1234yf with cooling water at 15 °C (T_7 and T_{15}).
- a5: R1234zez with cooling water at 15 °C (T_7 and T_{15}).
- a6: R1233zd with cooling water at 30 °C (T_7 and T_{15}).
- a7: R1244yd with cooling water at 30 °C (T_7 and T_{15}).
- a8: R1336mzz and 30 °C of cooling water (T_7 and T_{15}).
- a9: R1234yf and 27 °C of cooling water (T_7 and T_{15}).
- a10: R1234zez and 30 °C of cooling water (T_7 and T_{15}).

The objective of these cases is to examine the impact of varying refrigerant combinations on the system's performance objectives. Each case is optimized individually, thereby facilitating a comprehensive comparison across different fluid pairings.

In each case, the NSGA-II algorithm within pymoo is configured with a population size of 100. The algorithm employs reference directions generated using the Das–Dennis method, thereby ensuring a comprehensive and well-distributed search across the three-dimensional objective space. The optimization process is conducted over 100 generations, during which the population is refined to converge on a set of non-dominated solutions that offer optimal trade-offs between maximizing the COP and minimizing the compressor's pressure ratio.

The combination of the pymoo library and custom ORC-VCC system modeling provides a robust and adaptable framework for this study. pymoo's capabilities in handling multi-objective problems make it an ideal choice, particularly given the complex, non-linear relationships between the decision variables and the objectives. The custom code ensures that the thermodynamic and operational characteristics of the ORC-VCC system are accurately captured, thus allowing for precise evaluations of each candidate solution. This integrated approach allows for a thorough exploration of the design space, thus leading to the identification of refrigerant combinations and system configurations that optimize the critical objectives. The findings are expected to provide valuable insights into the design and operational strategies of ORC-VCC systems in energy recovery and cooling applications.

A comprehensive significance analysis is conducted to identify the key variables influencing the performance of the ORC-VCC system. Initially, relevant features are selected by excluding non-essential parameters to focus on the most impactful factors. Both the input variables and the target outcomes are standardized to ensure uniformity and to facilitate accurate comparisons. Linear regression models are then employed to assess the

relationships between the standardized features and each target variable, including the COP, the net power output, the cooling capacity, the pressure ratio, and the ORC efficiency. By analyzing the absolute values of the regression coefficients, the significance of each feature is determined, highlighting those with the most substantial effects on system performance. The analysis is performed using Python libraries, such as pandas for data manipulation, NumPy for numerical operations, scikit-learn for implementing the regression models, and seaborn for data visualization.

3. Results and Discussion

The optimization process yielded 130,000 calculation outputs from 10 independent optimization runs. Of these results, 77,516 were deemed suitable after data cleaning, with 29 key variables stored for further analysis. These optimizations, which evaluated various system configurations and parameter settings, provided insights into the system's behavior and performance under different conditions, ultimately supporting the identification of optimal solutions for the ORC-VCC system.

The distribution of decision variables offers a comprehensive understanding of the manner in which the parameters were explored during the optimization runs (Figure 7). The histograms demonstrate that several variables, including x_1, x_2, x_5, and x_6, exhibit a right-skewed distribution, indicating that lower values were more frequently selected as optimal settings. In contrast, other variables, such as x_4, exhibit a more uniform distribution across their ranges, indicating a less pronounced preference for particular values. It is noteworthy that x_9 and x_{10} demonstrate a uniform distribution, with a relatively balanced selection across their respective ranges. In contrast, x_7 and x_8 are predominantly concentrated around lower values, indicating a limited exploration of higher values. The distributions of x_{11} and x_{12} also indicate variability, reflecting the influence of system constraints. These distributions provide key insights into parameter sensitivity, highlighting how different design variables impact system performance and where further optimization may be possible.

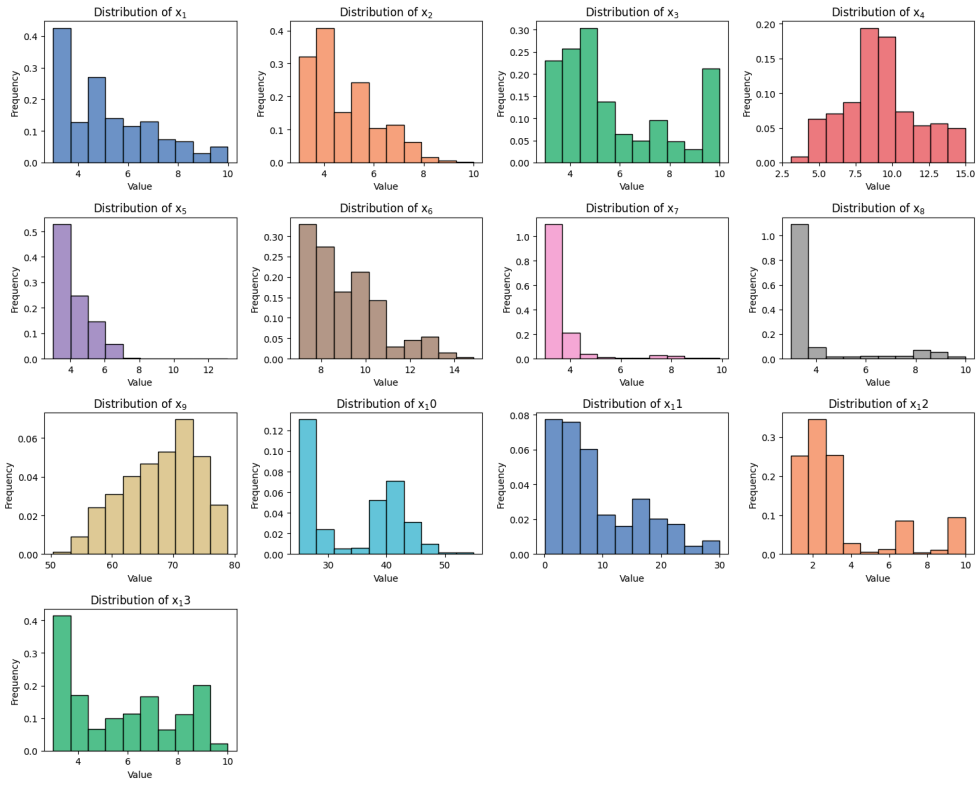

Figure 7. The frequency distribution of decision variables in the optimization runs.

Figures 8–12 illustrate the relationship between net power output, the coefficient of performance, and cooling generation for different refrigerants at a cooling water temperature of 15 °C. The data points are color-coded, with warmer colors (red) representing higher cooling capacities and cooler colors (blue) indicating lower capacities. The dataset, which includes all refrigerants (R1233zd, R1244yd, R1336mzz, R1234yf, and R1234ze), demonstrates an inverse relationship between the COP and the net power output. As the net power increases, the COP tends to decrease, indicating a trade-off between efficiency and power production. This behavior highlights the challenge of balancing both performance metrics to achieve an optimal design. Each refrigerant displays distinctive performance characteristics. For example, R1233zd and R1244yd exhibit relatively high coefficient of performance (COP) values at lower power outputs, making them well-suited to systems that prioritize efficiency over power. In contrast, R1234ze achieves higher cooling generation with a balanced trade-off between COP and power, making it a versatile option for mixed operational goals. Furthermore, the data offer insights into the maximum cooling generation achieved for each refrigerant. Both R1233zd and R1244yd achieve a maximum cooling generation of 400 kW, while R1336mzz reaches a slightly lower peak of approximately 350 kW. It is noteworthy that R1234yf and R1234ze attain even higher maximum cooling generation values of approximately 500 kW and 400 kW, respectively. These values indicate that R1234yf has the highest cooling generation capacity among the tested refrigerants, making it particularly suitable for applications focused on maximizing cooling output. The data also demonstrate the variability in cooling generation across different refrigerants. R1234yf exhibits a more uniform distribution of cooling capacities across varying power and COP combinations, whereas R1336mzz displays a more pronounced decline in cooling generation as the power increases. This comparison further elucidates the differences in refrigerant performance, thereby guiding the selection based on specific system requirements for cooling output, efficiency, and power trade-offs.

Figures 13–17 illustrate the relationship between the net power output, the COP, and cooling generation for different refrigerants at cooling water temperatures of 27 °C and 30 °C. It is noteworthy that a cooling water temperature of 27 °C represents the highest temperature achieved within the assumed constraints of this study. This boundary condition emphasizes the operational challenges posed by increasing temperatures and demonstrates the refrigerants' performance under these stringent conditions. Each refrigerant demonstrates unique performance characteristics. For example, R1233zd and R1244yd exhibit relatively high COP values at lower power outputs, making them ideal for applications that prioritize efficiency over power. In contrast, R1234ze achieves higher cooling generation while maintaining a balanced trade-off between COP and power, making it a versatile choice for systems with mixed operational objectives. Additionally, the data offer insights into the maximum cooling generation achieved for each refrigerant. R1233zd and R1234yf attain a maximum cooling generation of 200 kW, while R1244yd, R1234ze, and R1336mzz achieve slightly lower peaks, with values of approximately 175 kW, 175 kW, and 160 kW, respectively. The data also demonstrate the variability in cooling generation across different refrigerants. R1234yf exhibits a more uniform distribution of cooling capacities across varying power and COP combinations, whereas R1336mzz demonstrates a more pronounced decline in cooling generation as the power increases. This comparison highlights the differences in refrigerant performance, thus aiding the selection process based on specific system requirements for cooling output, efficiency, and power trade-offs.

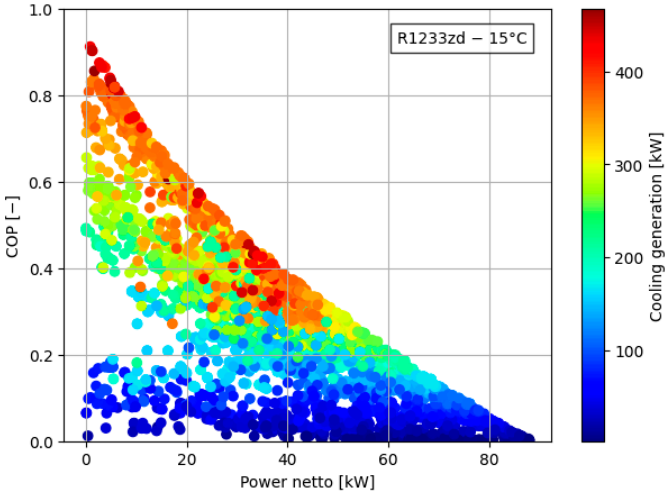

Figure 8. Relationship between COP, net power output, and cooling generation for R1233zd at 15 °C cooling water temperature.

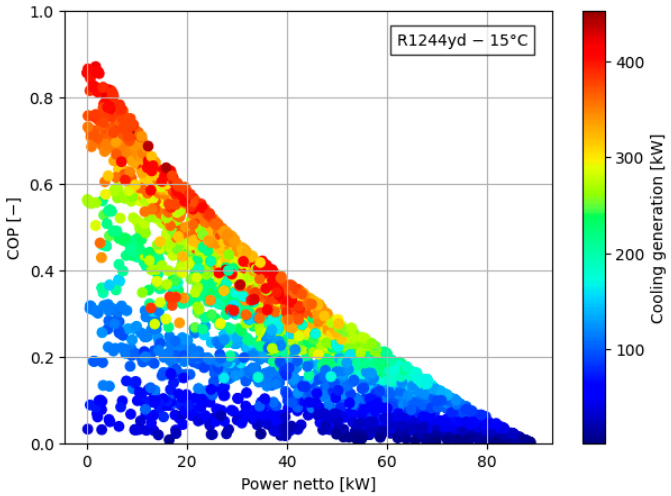

Figure 9. Relationship between COP, net power output, and cooling generation for R1244yd at 15 °C cooling water temperature.

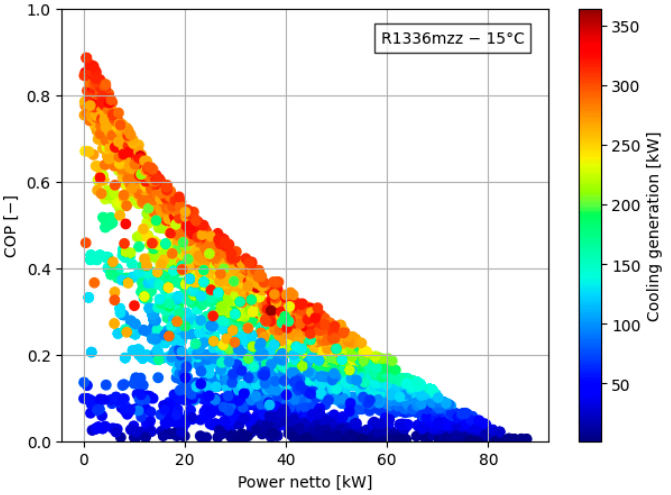

Figure 10. Relationship between COP, net power output, and cooling generation for R1336mzz at 15 °C cooling water temperature.

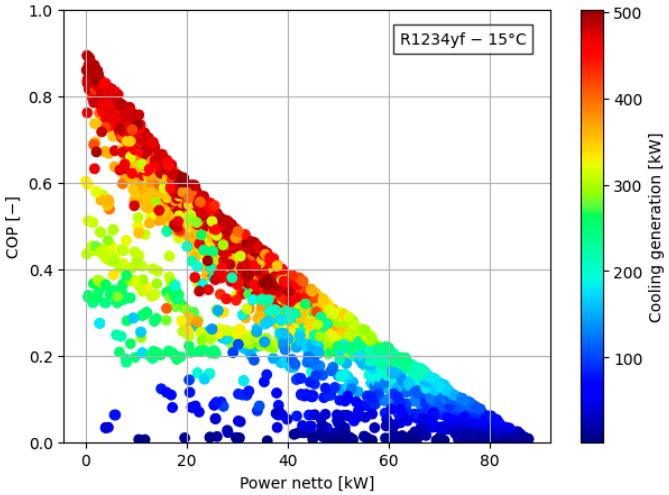

Figure 11. Relationship between COP, net power output, and cooling generation for R1234yf at 15 °C cooling water temperature.

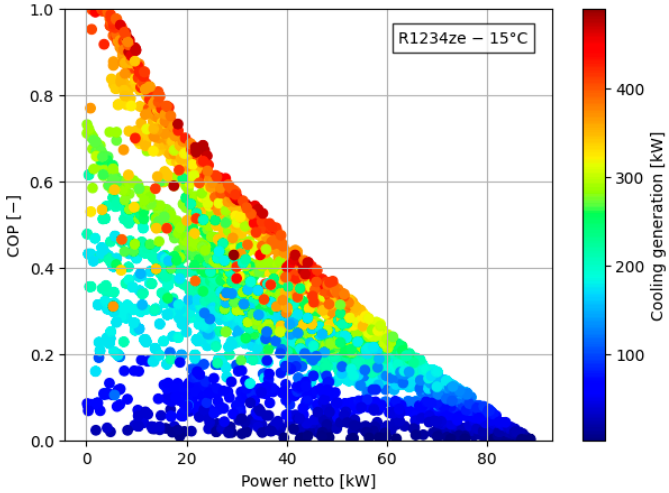

Figure 12. Relationship between COP, net power output, and cooling generation for R1234ze at 15 °C cooling water temperature.

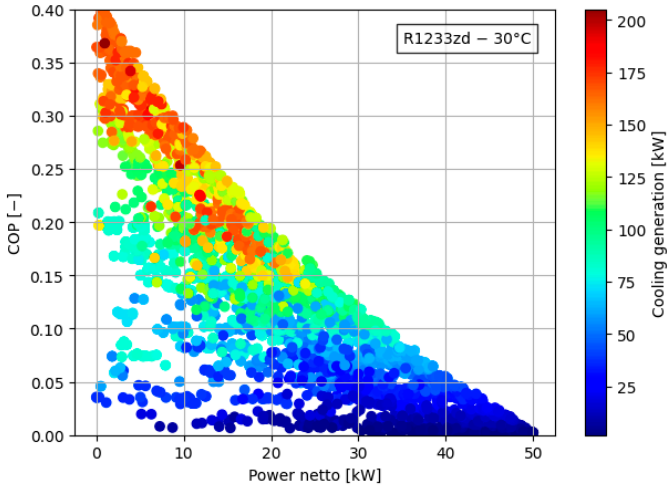

Figure 13. Relationship between COP, net power output, and cooling generation for R1233zd at 30 °C cooling water temperature.

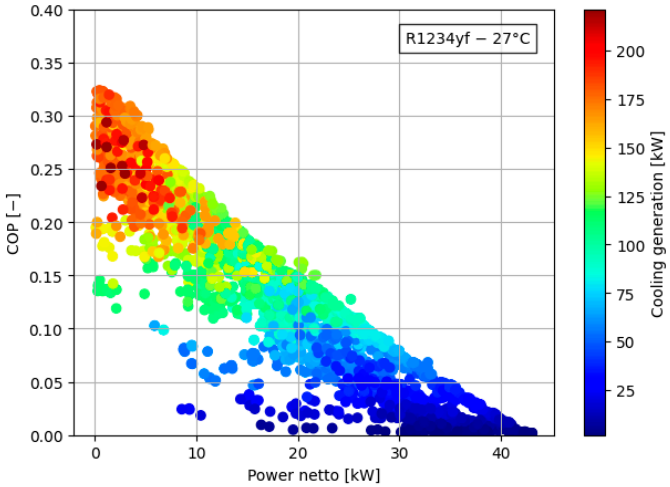

Figure 14. Relationship between COP, net power output, and cooling generation for R1234yf at 27 °C cooling water temperature.

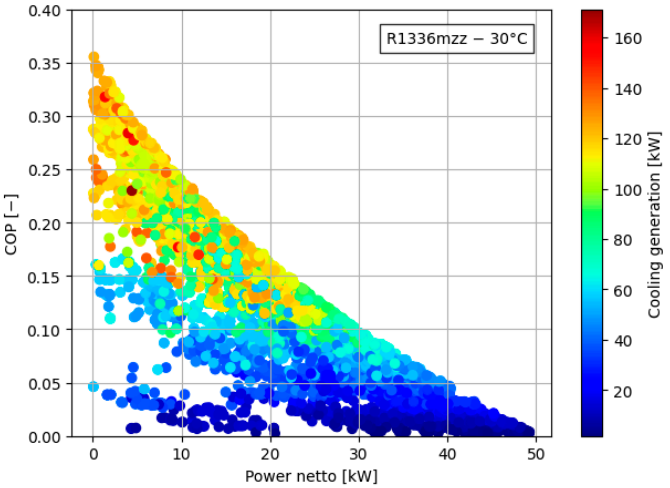

Figure 15. Relationship between COP, net power output, and cooling generation for R1336mzz at 30 °C cooling water temperature.

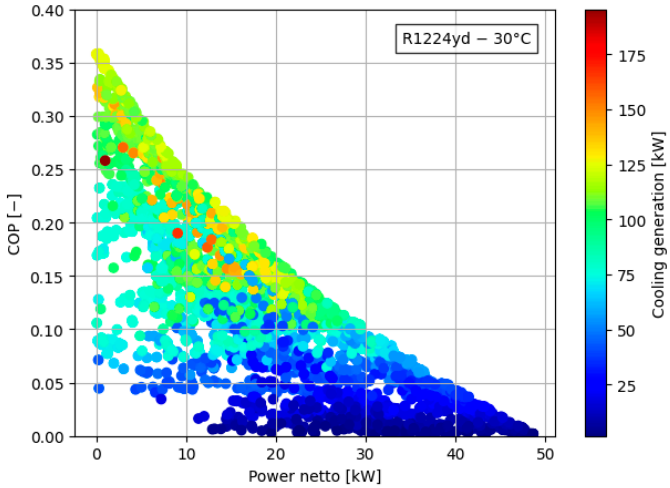

Figure 16. Relationship between COP, net power output, and cooling generation for R1224yd at 30 °C cooling water temperature.

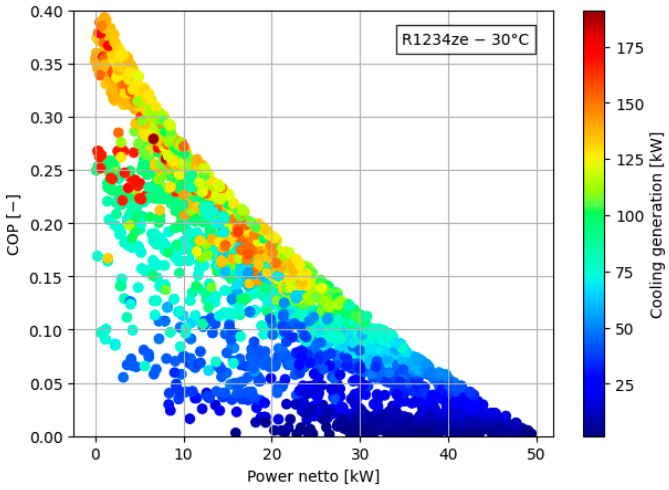

Figure 17. Relationship between COP, net power output, and cooling generation for R1234ze at 30 °C cooling water temperature.

Figure 18 depicts data for a cooling water temperature of 15 °C, wherein the COP attains elevated values, reaching a maximum of approximately 1.0 for R1234ze at lower net power outputs. The general trend illustrated in this figure demonstrates that as the net power output increases from 0 to approximately 90 kW, the coefficient of performance exhibits a gradual decline for all refrigerants under consideration. Among the refrigerants tested, R1234ze consistently exhibits a higher coefficient of performance across the range of power outputs, indicating a higher level of efficiency. The remaining refrigerants, including R1233zd, R1244yd, R1234yf, and R1336mzz, demonstrate a comparable pattern but attain lower maximum COP values, particularly at elevated net power outputs. This indicates that R1234ze is particularly well-suited to attaining high efficiency at low power outputs when operating with a cooling water temperature of 15 °C.

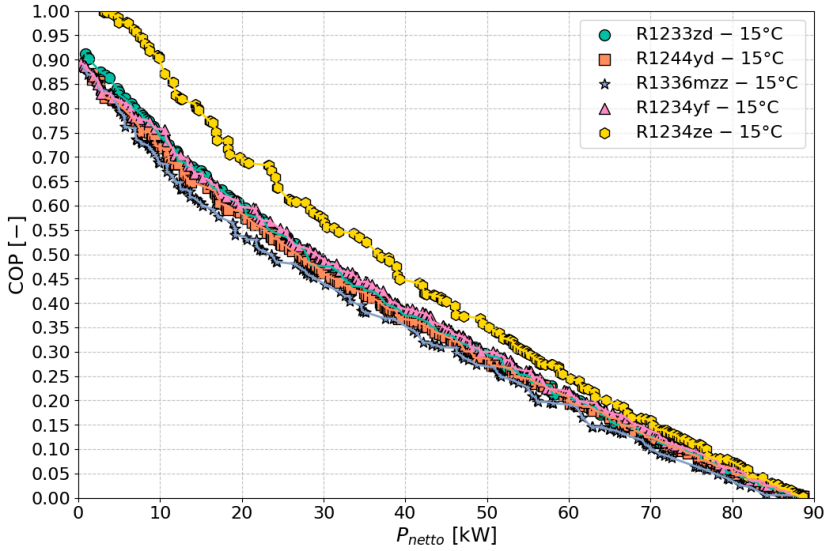

Figure 18. Pareto Frontier for different fluids at 15 °C cooling water temperature.

In contrast, Figure 19 depicts the performance of the same refrigerants at elevated cooling water temperatures (specifically, 27 °C and 30 °C). In this instance, the maximum COP values are markedly diminished, with a maximum of approximately 0.4. The decline in the COP with rising net power output is more pronounced than in the 15 °C scenario. Furthermore, the refrigerants demonstrate comparable performance across the power output range, exhibiting less discernible differentiation between them than in the initial figure. R1234yf, which attained a high COP at lower temperatures (Figure 18), exhibits diminished efficiency at elevated temperatures, indicating sensitivity to the cooling water temperature.

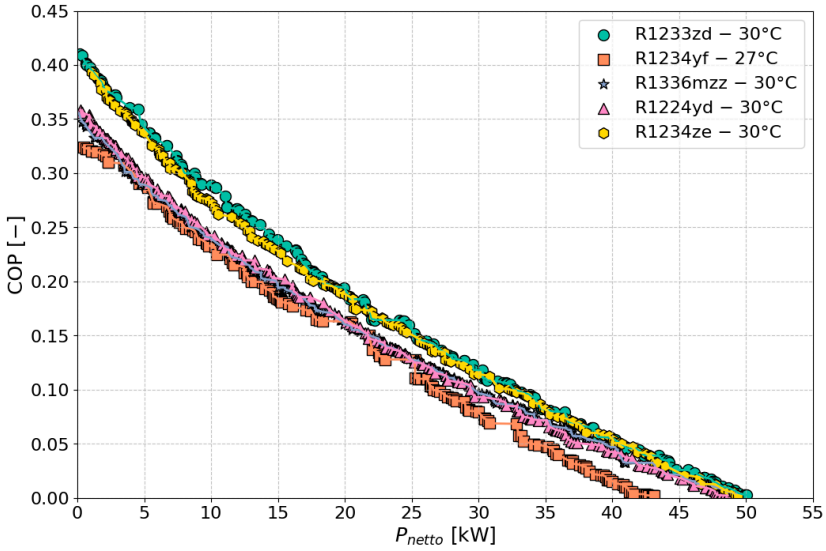

Figure 19. Pareto Frontier for different fluids at 30 °C cooling water temperature.

A comparison of the two figures reveals a notable discrepancy in the overall COP values. The second figure, representing a cooling water temperature of 30 °C, exhibits a markedly lower COP than the first figure, which depicts a cooling water temperature of 15 °C. This observation underscores the pivotal influence of the cooling water temperature on system efficiency. Furthermore, the range of achievable power outputs is diminished in the second figure, with a maximum of approximately 50 kW compared to approximately 90 kW in the first. This reduction in both the COP and the net power output highlights the challenges of achieving efficient operation at higher ambient temperatures. The results demonstrate that both the efficiency and the operational limits of the system are significantly influenced by the cooling water temperature. Refrigerants like R1234ze are more capable of maintaining higher COP values in favorable conditions (lower cooling water temperature).

Figures 20 and 21 illustrate the efficiency of the Organic Rankine Cycle (ORC) as a function of the net generated power. In both figures, a similar trend is observed: the efficiency is higher at lower power outputs and decreases as the generated power increases. This behavior is primarily due to the increasing power required to operate the ORC system's feed pump. Furthermore, the system often operates at higher condensation temperatures at increased power levels, necessitating a greater amount of heat to be rejected in the ORC condenser. Collectively, these factors contribute to a reduction in the overall Coefficient of Performance (COP) of the system.

Figures 22 and 23 illustrate the correlation between the coefficient of performance (COP) and the net power output for the refrigerant R1233zd, emphasizing the impact of the pressure ratio (Figure 22) and cooling generation (Figure 23). In the initial figure, the color coding for the pressure ratio demonstrates a slight increase from approximately 3.85 to 4.20 as the power output rises, indicating that a higher power output may result in an elevated pressure ratio, which could potentially diminish efficiency. In contrast, the second figure demonstrates a more pronounced variability in cooling generation, with higher COP values corresponding to higher cooling capacities and vice versa. A notable conclusion

from comparing these figures is that a lower pressure ratio can be achieved with lower cooling generation, indicating that optimizing for reduced mechanical stress may require sacrificing cooling capacity. This observation highlights the inherent trade-offs in system design when attempting to balance power output, efficiency, and cooling performance. Figure 24 demonstrates the outlet pressure from the VCC compressor. For the working fluid R1233zd, the outlet pressure remains relatively low, oscillating between 2.1 and 2.3 bar. A comparable range of percentage deviations for this parameter is observed among the other analyzed working fluids. This consistency in outlet pressure variations indicates a stable performance of the VCC compressor across different refrigerants.

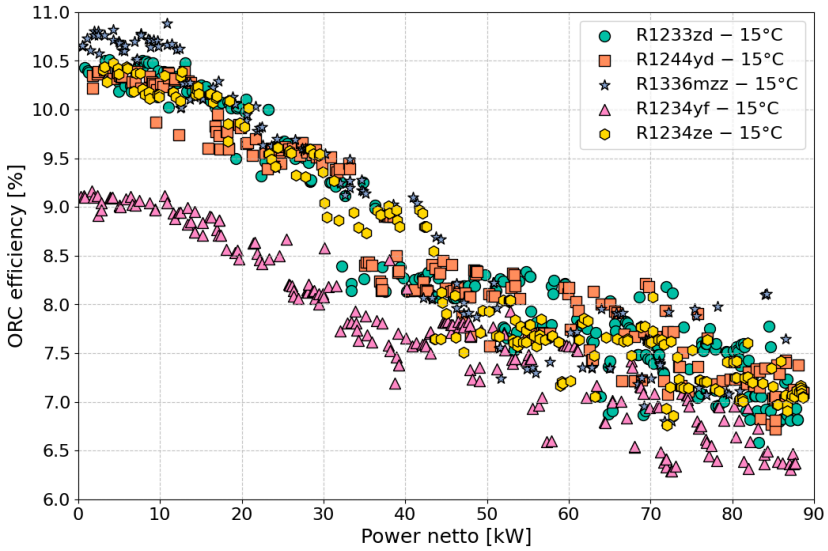

Figure 20. Comparison of ORC efficiency versus net power output for various working fluids at a cooling water temperature of 15 °C.

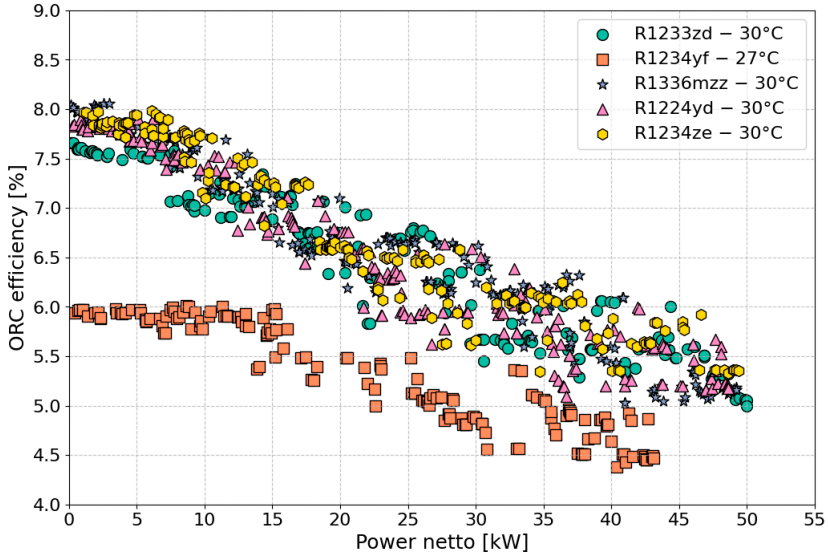

Figure 21. Comparison of ORC efficiency versus net power output for various working fluids at a cooling water temperature of 30 °C.

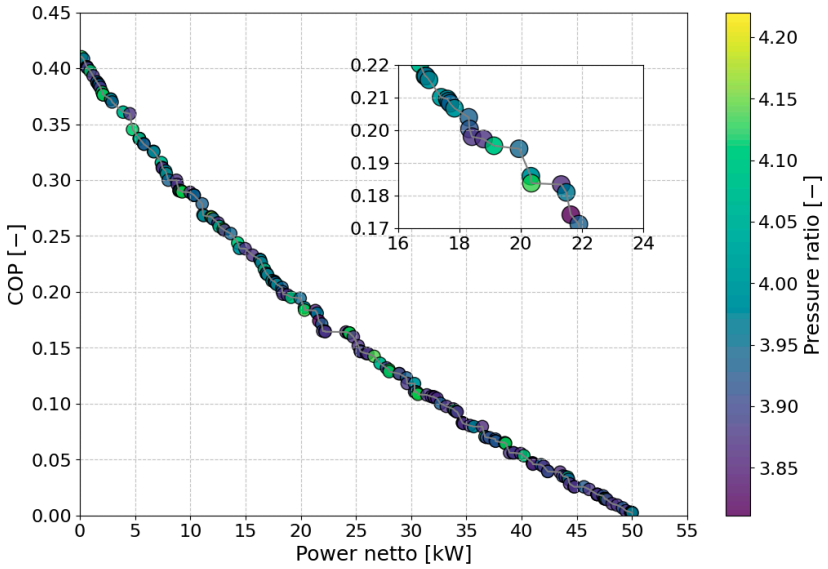

Figure 22. Relationship between COP, net power output, and pressure ratio for R1233zd at 30 °C cooling water temperature.

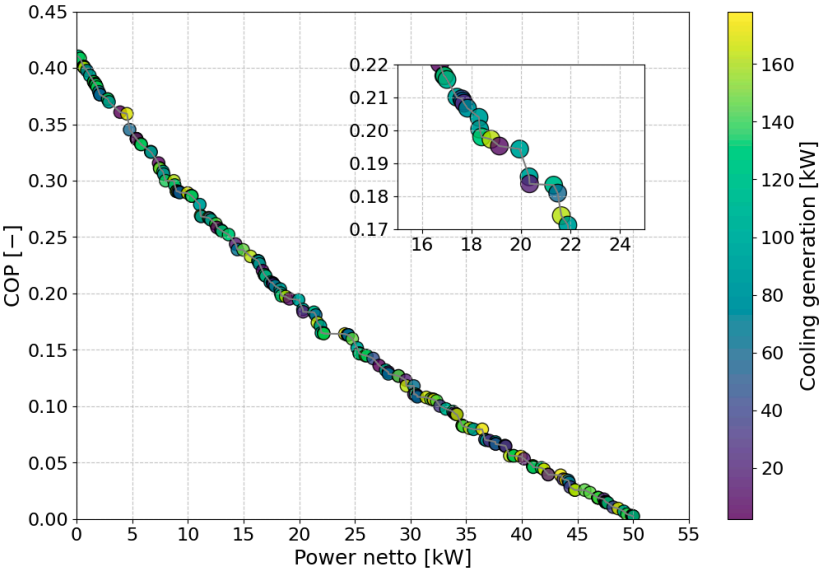

Figure 23. Relationship between COP, net power output, and cooling generation for R1233zd at 30 °C cooling water temperature.

Figure 25 provides a summary of the significance of the objective function variables, emphasizing their correlations with key performance indicators, including the COP, the net power output (P_{netto}), cooling generation ($Q_{cooling}$), the pressure ratio (PR), and ORC efficiency (η_{orc}). The color gradient represents the magnitude of the correlation, with darker shades of blue indicating stronger positive correlations and lighter shades indicating weaker relationships. The variables x_9, x_{10}, and x_{11} exert the most significant influence on system performance. In particular, x_{11} demonstrates a pronounced positive correlation (0.77 to 1.00) with cooling generation and ORC efficiency, indicating its pivotal role in optimizing these metrics. Similarly, variables x_9 and x_{10} exert a considerable influence on the net power output, cooling generation, and the pressure ratio, with correlation coefficients ranging from 0.48 to 0.89. These variables are of great consequence in determining both power and efficiency outcomes. In contrast, variables x_1 through x_8 exhibit minimal correlations with the objective functions, indicating that they exert a limited influence on overall system

performance. The relatively low values across these variables indicate that they may not be as critical for optimizing the COP, the power output, or the cooling capacity. Due to the pronounced influence of decision variable x_{11} on the $Q_{cooling}$, an additional analysis was conducted excluding x_{11}. The results of this analysis indicate that variable x_{10} (saturation temperature in the ORC condenser) has the most significant impact (Figure 26). Variable x_{10} directly affects the turbine's lower expansion temperature, which consequently leads to a greater enthalpy drop in the turbine and increased turbine power at the same mass flow rate. Higher turbine power enables greater compressor power, ultimately enhancing the cooling capacity. The results inform which variables exert a significant influence on the system's performance. This allows for more targeted optimization whereby influential variables are given priority, thus enhancing both computational efficiency and the quality of the optimized design.

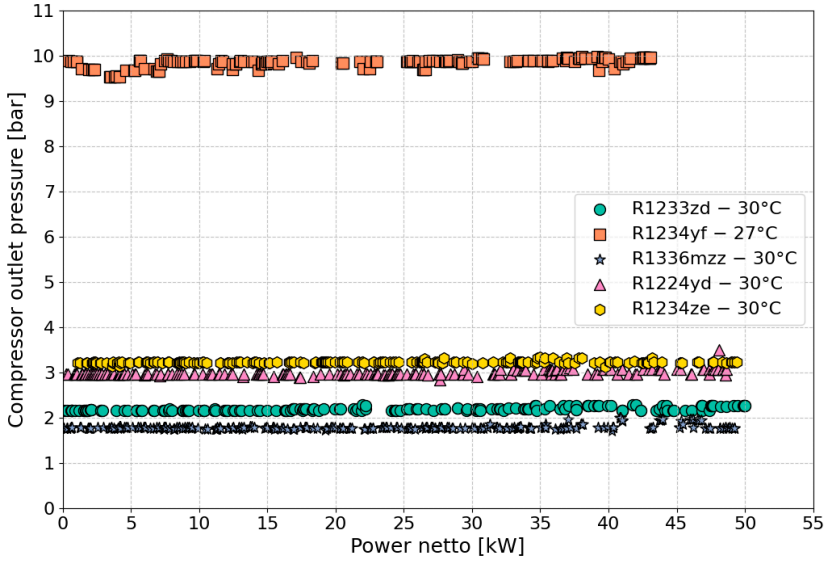

Figure 24. Comparison of compressor outlet pressure versus net power output for various working fluids at a cooling water temperature of 30 °C.

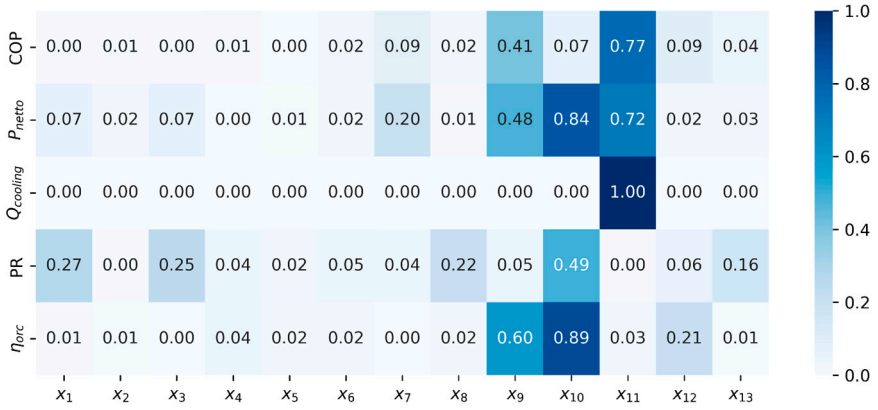

Figure 25. Summary of significance of the objective functions variables.

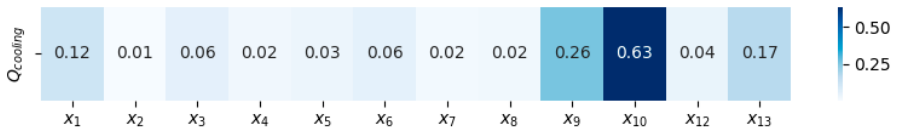

Figure 26. Influence of decision variables on cooling generation.

4. Conclusions

This study presents a comprehensive optimization of an ORC-VCC system designed for electricity and cooling production from low-grade waste heat, with a particular focus on five different refrigerants and two distinct cooling water temperatures. The results demonstrate the potential of ORC-VCC technology to achieve high efficiency, with overall cycle efficiencies exceeding 90%. This underlines the suitability of ORC-VCC technology for waste heat recovery applications. The optimization runs revealed significant trade-offs between the COP, the net power output, and cooling generation. This highlights the importance of selecting appropriate working fluids and design parameters to meet specific operational goals.

The findings of this research demonstrate the efficacy of employing advanced multi-objective optimization techniques, such as NSGA-II, to navigate the intricate solution space and discern optimal trade-offs between competing objectives. The insights gained from this study provide valuable guidance for the design and deployment of ORC-VCC systems, thereby contributing to the development of sustainable, energy-efficient technologies capable of mitigating the environmental impact of increased cooling demands in a warming world. Future work will concentrate on the optimization of the code, which will be extended to include the 0D design of turbochargers. Furthermore, the objective function will be expanded to encompass key variables relevant to turbocharger design, with the objective of enhancing the system's performance and integration potential in a wider range of applications.

Furthermore, the objective is to scale the technology to broader industrial applications, with a particular focus on certain sectors, such as manufacturing, transportation, and energy-intensive industries, where low-grade waste heat is abundant. The integration of these systems will contribute to a reduction in carbon emissions, an improvement in energy utilization, and the creation of cost-effective solutions for energy production and cooling.

In conclusion, the objective of this study was to develop a highly adaptable ORC-VCC system that can be effectively implemented across diverse applications, thereby assisting industries in their transition towards more sustainable practices. By optimizing both the ORC and the turbocharger components, the system's ability to maximize energy recovery from waste heat and minimize environmental impacts can be significantly enhanced, thus paving the way for next-generation energy solutions in a resource-constrained world.

Funding: This research was supported by the National Centre for Research and Development (NCBR) through the LIDER XIV programme within the COOLERHEAT project (Grant Agreement Number LIDER14/0173/2023).

Data Availability Statement: The original contributions of this study are included in the article; further inquiries can be directed to the corresponding author.

Conflicts of Interest: The authors declare no conflicts of interest.

References

1. NASA Earth Observatory. Available online: https://earthobservatory.nasa.gov/features/GlobalWarming (accessed on 5 September 2024).
2. International Energy Agency IEA. Available online: https://www.iea.org/data-and-statistics/charts/growth-in-global-air-conditioner-stock-1990-2050 (accessed on 29 September 2024).
3. Forman, C.; Muritala, I.K.; Pardemann, R.; Meyer, B. Estimating the Global Waste Heat Potential. *Renew. Sustain. Energy Rev.* **2016**, *57*, 1568–1579. [CrossRef]
4. Tocci, L.; Pal, T.; Pesmazoglou, I.; Franchetti, B. Small Scale Organic Rankine Cycle (ORC): A Techno-Economic Review. *Energies* **2017**, *10*, 1–26. [CrossRef]
5. Linke, P.; Papadopoulos, A.I.; Seferlis, P. Systematic Methods for Working Fluid Selection and the Design, Integration and Control of Organic Rankine Cycles-A Review. *Energies* **2015**, *8*, 4775–4801. [CrossRef]
6. Saeed, M.Z.; Contiero, L.; Blust, S.; Allouche, Y.; Hafner, A.; Eikevik, T.M. Ultra-Low-Temperature Refrigeration Systems: A Review and Performance Comparison of Refrigerants and Configurations. *Energies* **2023**, *16*, 7274. [CrossRef]
7. Tassou, S.A.; Lewis, J.S.; Ge, Y.T.; Hadawey, A.; Chaer, I. A Review of Emerging Technologies for Food Refrigeration Applications. *Appl. Therm. Eng.* **2010**, *30*, 263–276. [CrossRef]

8. Pan, M.; Zhao, H.; Liang, D.; Zhu, Y.; Liang, Y.; Bao, G. A Review of the Cascade Refrigeration System. *Energies* **2020**, *13*, 2254. [CrossRef]
9. Bahrami, M.; Pourfayaz, F.; Kasaeian, A. Low Global Warming Potential (GWP) Working Fluids (WFs) for Organic Rankine Cycle (ORC) Applications. *Energy Rep.* **2022**, *8*, 2976–2988. [CrossRef]
10. Kumar, A.; Rakshit, D. A Critical Review on Waste Heat Recovery Utilization with Special Focus on Organic Rankine Cycle Applications. *Clean. Eng. Technol.* **2021**, *5*, 100292. [CrossRef]
11. Witanowski, Ł. Comprehensive Analysis of ORC-VCC System for Air Conditioning from Low-Temperature Waste Heat. In Proceedings of the 7th International Seminar on ORC Power System (ORC 2023), Seville, Spain, 4 September 2023; pp. 203–213.
12. Khatoon, S.; Almefreji, N.M.A.; Kim, M.H. Thermodynamic Study of a Combined Power and Refrigeration System for Low-Grade Heat Energy Source. *Energies* **2021**, *14*, 410. [CrossRef]
13. Elbir, A.; Kodaloglu, F.; Ucgul, I.; Sahin, M. Thermodynamic Analysis of Refrigerants Used in ORC-VCC Combined Power Systems for Low Temperature Heat Sources. *Therm. Sci.* **2022**, *26*, 2855–2863. [CrossRef]
14. Wang, H.; Peterson, R.; Herron, T. Design Study of Configurations on System COP for a Combined ORC (Organic Rankine Cycle) and VCC (Vapor Compression Cycle). *Energy* **2011**, *36*, 4809–4820. [CrossRef]
15. Bao, J.; Zhang, L.; Song, C.; Zhang, N.; Zhang, X.; He, G. Comparative Study of Combined Organic Rankine Cycle and Vapor Compression Cycle for Refrigeration: Single Fluid or Dual Fluid? *Sustain. Energy Technol. Assess.* **2020**, *37*, 100595. [CrossRef]
16. Marion, M.; Louahlia, H. Volumetric Design for ORC-VCC Compressor-Expander Units. *Int. J. Refrig.* **2021**, *132*, 1–10. [CrossRef]
17. Toujani, N.; Bouaziz, N.; Chrigui, M.; Kairouani, L. The Impact of Operating Parameters on the Performance of a New ORC–VCC Combination for Cogeneration. *Therm. Eng.* **2020**, *67*, 660–672. [CrossRef]
18. Kim, M.-H. Energy and Exergy Analysis of Solar Organic Rankine Cycle Coupled with Vapor Compression Refrigeration Cycle. *Energies* **2022**, *15*, 5603. [CrossRef]
19. Karellas, S.; Braimakis, K. Energy-Exergy Analysis and Economic Investigation of a Cogeneration and Trigeneration ORC-VCC Hybrid System Utilizing Biomass Fuel and Solar Power. *Energy Convers. Manag.* **2016**, *107*, 103–113. [CrossRef]
20. Nasir, M.T.; Kim, K.C. Working Fluids Selection and Parametric Optimization of an Organic Rankine Cycle Coupled Vapor Compression Cycle (ORC-VCC) for Air Conditioning Using Low Grade Heat. *Energy Build.* **2016**, *129*, 378–395. [CrossRef]
21. Alshammari, S.; Kadam, S.T.; Yu, Z. Assessment of Single Rotor Expander-Compressor Device in Combined Organic Rankine Cycle (ORC) and Vapor Compression Refrigeration Cycle (VCR). *Energy* **2023**, *282*, 128763. [CrossRef]
22. Grauberger, A.; Young, D.; Bandhauer, T. Experimental Validation of an Organic Rankine-Vapor Compression Cooling Cycle Using Low GWP Refrigerant R1234ze(E). *Appl. Energy* **2022**, *307*, 118242. [CrossRef]
23. Grauberger, A.; Young, D.; Bandhauer, T. Off-Design Performance of an Organic Rankine-Vapor Compression Cooling Cycle Using R1234ze(E). *Appl. Energy* **2022**, *321*, 119421. [CrossRef]
24. Sleiti, A.K.; Al-Ammari, W.A.; Al-Khawaja, M. Experimental Investigations on the Performance of a Thermo-Mechanical Refrigeration System Utilizing Ultra-Low Temperature Waste Heat Sources. *Alex. Eng. J.* **2023**, *71*, 591–607. [CrossRef]
25. Blank, J.; Deb, K. Pymoo: Multi-Objective Optimization in Python. *IEEE Access* **2020**, *8*, 89497–89509. [CrossRef]
26. Deb, K.; Jain, H. An Evolutionary Many-Objective Optimization Algorithm Using Reference-Point-Based Nondominated Sorting Approach, Part I: Solving Problems with Box Constraints. *IEEE Trans. Evol. Comput.* **2014**, *18*, 577–601. [CrossRef]
27. Jain, H.; Deb, K. An Evolutionary Many-Objective Optimization Algorithm Using Reference-Point Based Nondominated Sorting Approach, Part II: Handling Constraints and Extending to an Adaptive Approach. *IEEE Trans. Evol. Comput.* **2014**, *18*, 602–622. [CrossRef]
28. Deb, K.; Pratap, A.; Agarwal, S.; Meyarivan, T. A Fast and Elitist Multiobjective Genetic Algorithm: NSGA-II. *IEEE Trans. Evol. Comput.* **2002**, *6*, 182–197. [CrossRef]
29. Aram, K.; Taherkhani, R.; Šimelytė, A. Multistage Optimization toward a Nearly Net Zero Energy Building Due to Climate Change. *Energies* **2022**, *15*, 983. [CrossRef]
30. Wang, L.; Yang, J.; Qu, B.; Pang, C. Multi-Objective Optimization of an Organic Rankine Cycle (ORC) for a Hybrid Solar–Waste Energy Plant. *Energies* **2024**, *17*, 1810. [CrossRef]
31. Aieneh, K.; Mehranfar, S.; Yazdi Sotoude, M.; Sadeghi, S.; Mahmoudzadeh Andwari, A. Solar-Powered Combined Cooling, Heating, and Power Energy System with Phase-Change Material and Water Electrolysis: Thermo-Economic Assessment and Optimization. *Energies* **2024**, *17*, 3309. [CrossRef]
32. Wang, X.; Chen, X.; Xing, C.; Ping, X.; Zhang, H.; Yang, F. Performance Analysis and Rapid Optimization of Vehicle ORC Systems Based on Numerical Simulation and Machine Learning. *Energies* **2024**, *17*, 4542. [CrossRef]